Novel structural insights for a pair of monoclonal antibodies recognizing non-overlapping epitopes of the glucosyltransferase domain of *Clostridium difficile* toxin B

Jinyu Liu [a,*], Michael Kothe [a], Jianxin Zhang [b], Eliud Oloo [b,1], Svetlana Stegalkina [b], Sophia T. Mundle [b], Lu Li [b], Jinrong Zhang [b,3], Leah E. Cole [b], Lucianna Barone [b,4], Hans-Peter Biemann [a], Harry Kleanthous [b,5], Natalie G. Anosova [b], Stephen F. Anderson [b,2]

[a] *Sanofi Integrated Drug Discovery, 153 2nd Ave, Waltham, 02451, USA*
[b] *Sanofi Pasteur, 38 Sidney Street, Cambridge, MA, 02139, USA*

ARTICLE INFO

ABSTRACT

Clostridium difficile toxins are the primary causative agents for hospital-acquired diarrhea and pseudomembranous colitis. Numerous monoclonal antibodies (mAbs) targeting different domains of *Clostridium difficile* toxin have been reported. Here we report the crystal structures of two mAbs, B1 and B2, in complex with the glycosyltransferase domain (GTD) of the *Clostridium difficile* toxin B (TcdB). B2 bound to the N-terminal 4 helix bundle of the GTD, a conserved membrane localization domain (MLD) found in the large clostridial glycosylating toxin family implicated in targeting plasma membrane. B1 bound to a distinct epitope at the hinge region between the MLD and the catalytic subdomain of the GTD. Functional studies revealed the potency of these mAbs *in vitro* and *in vivo* to be synergistic when given in combination.

1. Introduction

Clostridium difficile (recently proposed for reclassification as *Clostridioides difficile*) (Lawson et al., 2016) is the etiological agent responsible for *C. difficile*-associated diarrhea (CDAD). In the US, a recent survey by the Centers for Disease Control estimated a burden of 159,700 community-acquired and 293,300 healthcare-associated infections per year, killing an estimated 29,300 within 30 days of diagnosis *of C. difficile* infection (CDI) (Lessa et al., 2015). Low levels of *C. difficile* can be a normal part of the gut flora (Testore et al., 1986), and asymptomatic *C. difficile* colonization prevalence has been calculated to be between 0 and 15% in various studies (Furuya-Kanamori et al., 2015). *C. difficile* is a spore-forming bacterium (Hall and O'Toole, 1935) and when the gut microbiome is perturbed by antibiotics, *C. difficile* spores from asymptomatic colonization or encountered through novel and frequently

nosocomial exposure, can germinate into vegetative cells which can outcompete the other gut flora (Peterfreund et al., 2012). Vegetative cells produce two large, secreted virulence factors, toxins A (TcdA) and B (TcdB). These two toxins can enter the epithelial cells of the colon and cause loss of intestinal membrane integrity, fluid secretion, inflammation, and cell death.

TcdA and TcdB are multi-functional proteins with similar domain architecture and about 49% shared identity at the amino acid level (von Eichel-Streiber et al., 1996). Both proteins consist of an N-terminal GTD which is responsible for transferring glucose from UDP-glucose to the switch I region of the Rho-family of small GTPases (Just et al., 1995), a cysteine protease domain (CPD) which autocatalytically releases the N-terminal toxin domain into the cytosol (Reineke et al., 2007), a translocation domain (TLD) which rearranges to form a pore through which the toxin domain is threaded into the cytosol (Zhang et al., 2014),

and a C-terminal receptor-binding domain (RBD) which consists of multiple repeated structures called CROPs (Combined Repetitive Oligo-Peptides) (Olling et al., 2011) that function in the attachment of the toxin to the host cell surface. Additionally, TcdB has been shown capable of binding to cells using non-CROP regions in the TLD (Yuan et al., 2015; Manse and Baldwin, 2015; Genisyuerek et al., 2011).

A key step of intoxication process for TcdB and TcdA is the glycosylation of Rho-family small GTPases. Upon the release of toxin domain into the cytosol, Rho proteins are inactivated. Rho proteins are involved in many biological processes and signaling pathways. The inactivation of Rho proteins leads to cytopathic and cytotoxic effects including actin reorganization, disruption of intracellular junctions, increased cell barrier permeability and increased expression of pro-apoptotic genes (Just et al., 1995). The small GTPases cycle between GTP-bound active and GDP-bound inactive forms. For example, Rho family GTPases cycle between active forms bound to the plasma membrane, and inactive forms which are linked to GDI (guanine nucleotide dissociation inhibitor) in the cytosol. Recent discoveries have revealed a N-terminal small domain consisting of a 4-helix bundle within the glucosyltransferase domain of TcdB plays key roles in plasma membrane localization. This membrane localization domain (MLD) within TcdB was identified as a conserved domain among numerous bacterial toxins including the large clostridial glucosylating toxin (LCGT) family (Geissler et al., 2012). Further studies established a model that residues in loop 1 between helix 1 and 2, in loop 3 between helix 3 and 4 in MLD are important for phosphatidyserine (PS) binding, membrane localization and GTPase catalysis (Chavez et al., 2015, 2016; Reinert et al., 2005).

Although early structural efforts involving the intact holotoxins were largely unsuccessful, the crystal structures of domains of both toxins have been solved by a number of laboratories. The crystal structure of the GTD of TcdA and TcdB have been solved, with its substrate UDP-glucose (Reinert et al., 2005; Pruitt et al., 2010), UDP and manganese (D'Urzo et al., 2012) and without substrates (Pruitt et al., 2010; D'Urzo et al., 2012). The crystal structure of the cysteine protease domain (CPD) of TcdB has been solved, with (Puri et al., 2010) and without inhibitors (Pruitt et al., 2009; Shen et al., 2011). A five-repeat fragment of the CTD of TcdA (Ho et al., 2005) has been crystallized and used to model the entire domain. Another fragment has been crystallized by Greco et al., bound to the trisaccharide Galα1,3Galβ1,4GlcNac, a presumed receptor of TcdA (Greco et al., 2006).

The quaternary arrangement of these domains was first proposed by Pruitt et al. based on electron microscopy (Pruitt et al., 2010), but a model based on small-angle x-ray scattering (Albesa-Jove et al., 2010) came to different conclusions, perhaps reflecting different preparation methods. A higher-resolution structure of the N-terminal domains (GTD, CPD, and TLD) by x-ray crystallography finally assigned the domains to their current locations (Chumbler et al., 2016). Structure determination by cryo-electon microscopy showed that the holotoxins are flexible and inhabit multiple conformations, of which, the crystal structure is presumed to be one of the more common (Pruitt et al., 2010). At pH 4.5, within the lysosome, a particularly drastic rearrangement of the toxin occurs which could serve to prepare the toxin for penetration of the membrane. The crystal structure of the full length TcdB holotoxin in complex with 3 nanobodies published by the Jin laboratory at UC Irvine finally revealed the relative orientations of all 4 functional domains (GTD, CPD, TLD and CROPs) at endosomal pH. This study displays an architecture that is distinct from that of the prior model derived from EM and highlighted the conformational dynamics of the CROPs domain at differential pH (Chen et al., 2019).

As part of the long-standing efforts of tackling CDAD by developing mAbs, structures of toxin neutralizing Fabs in complex with different domains of TcdA or TcdB have also been reported. These include the crystal structure of a Fab fragment of bezlotoxumab bound to the N-terminal half of the TcdB CROP domain (Orth et al., 2014), and the Fab fragment of actoxumab bound to a portion of the TcdA RBD (Hernandez et al., 2017). Murase et al. published structures of the RBDs of TcdA and

TcdB bound by neutralizing and non-neutralizing single-domain antibodies (Murase et al., 2014). Kroh et al. reported a crystal structure of two humanized mAb PA50 Fabs bound to a segment of the TcdA CROPs (Kroh et al., 2017). All of these antibodies bind to the CROP domain or the RBD, and blockage of cell surface binding was proposed to be the mechanism of action for neutralization.

Most recently, Kroh et al. reported a crystal structure of PA41 bound to a small subdomain of the GTD domain. Blockage of translocation and delivery of the enzyme cargo was thought to be the mechanism of action for neutralization (Kroh et al., 2018). Together with the structure of the full length TcdB holotoxin, Jin's group also published structures of 3 antibodies and among them, 7F and E3 were bound to the GTD domain (Chen et al., 2019). 7F binds to the C-terminal region of the GTD and inhibits toxin cleavage without interacting with the CPD directly. E3 binds to the side of the MLD and was reported to inhibit Rho glycosylation.

In our previous publication (Anosova et al., 2015), we described a pair of TcdB neutralizing mAbs which we mapped to the N-terminal GTD. These antibodies showed *C. difficile* TcdB neutralizing activity when tested alone, but when assessed in combination they were much more potent. In order to further characterize these important neutralizing mAbs, we co-crystallized Fab fragments made from these mAbs in complex with a recombinant TcdB-GTD. The resulting cocrystal structures allow us to confirm that mAbs B1 & B2 bind to novel non-overlapping epitopes of the TcdB-GTD. These data provide tantalizing structural insights for mAb B2 mechanism of action in neutralizing *C. difficile* TcdB. Furthermore, in-depth functional assessments of B1 & B2 mAbs and Fabs demonstrate a clear synergistic effect on neutralization of toxins when used in combination.

2. Results

2.1. X-ray structure of Fab B2 bound to TcdB-GTD

The TcdB-GTD B2 Fab complex (simplified as GTD-B2 complex below) crystallized in space group P2$_1$ with cell dimensions of a = 61.2, b = 110.7, c = 83.1, α = 90°, β = 99.3°, γ = 90°. The crystals diffracted to 1.8 Å resolution. The final model of GTD-B2 has an R$_{free}$ of 0.222 and R$_{factor}$ of 0.186 with good geometry and contains one molecule of GTD-B2 complex in each asymmetric unit (Fig. 1A and Table 4). The refined structure of the GTD-B2 complex encompasses residues 3–540 of the GTD, all residues of the B2 light chain, and all residues of the B2 heavy chain except for residues 136–141. The secondary structures of the GTD-B2 and representative electron density for regions and residues involved in interactions between GTD and B2 are identified in Fig. 1C and B respectively.

The B2 binding site is located at the tip of the MLD. B2 has an overall binding area of 537 Å^2 contributed by the heavy chain and 330 Å^2 contributed by the light chain. Residues involved in binding of B2 include residues 17–23 in loop 1 between helix 1 and helix 2 of the MLD, and residues 62–63 in loop 3 between helix 3 and helix 4 of the MLD (Fig. 1D). In loop 1, F17 forms a hydrophobic parallel interaction with Y53 from the heavy chain; residue D22 sticks into a pocket formed by the heavy and light chains, forming H-bond interactions with R100, R101and T108 of the heavy chain, and the side chain of D22 forms a hydrophobic interaction with Y54 from the light chain (Fig. 1D). Due to the extensive interactions between D22 and the heavy and light chains, this residue probably plays a critical role in the binding of B2. E23 forms a strong H-bond interaction with NH of A103 from the heavy chain and the OH group of Y37 from the light chain. Q20 of loop 1 forms a strong H-bond interaction with the backbone NH of R101 and the carbonyl group of E31 from the heavy chain. Interactions with Fab B2 in the loop 3 region involve T62 and Y63, where T62 forms an H-bond with N33 from the light chain and Y63 forms an H-bond with A103 and a van der Waals interaction with the R101 side chain (Fig. 1D).

For B2, residues 100–108 of the heavy chain seem to play a key role in
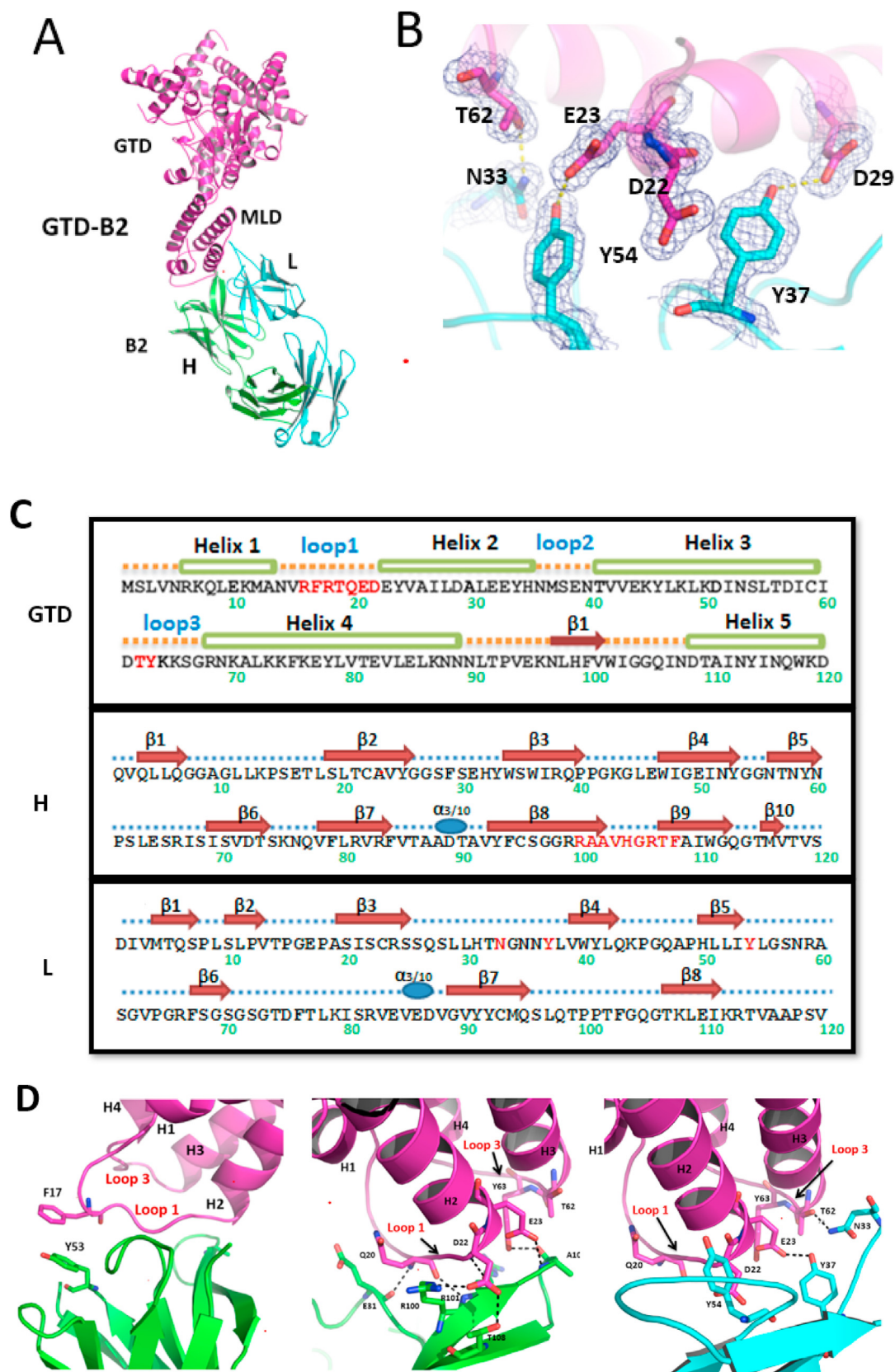
Fig. 1. Structure of TcdB GTD-B2. A: Crystal structure of TcdB GTD-B2. Heavy chain (H) and light chain (L) of B2 were shown in green and cyan respectively. GTD is shown in magenta and the N-terminal 4 α-helix bundle of GTD is labeled as MLD. B: 2Fo-Fc electron density contoured at 1.0σ for representative residues involved in interactions between L chain of B2 and MLD of GTD. C: Secondary structure schematic representation for GTD, H chain, L chain of B2 for regions involved in interactions. Residues involved in interactions are labeled in red. D: Detailed interactions between H and L chain of B2 and MLD of GTD. (For interpretation of the references to colour in this figure legend, the reader is referred to the Web version of this article.)

epitope recognition by interacting with the residues in loop 1 and 3. N33, Y37, and Y54 of the light chain are the residues involved in epitope recognition with loop 1 and loop 3 of GTD. Other interactions include Y53 of the heavy chain, which forms parallel hydrophobic interactions with F17 of loop 1, and E31 of the heavy chain that forms parallel van der Waals interactions with the side chain of Q20.

2.2. X-ray structure of Fab B1 bound to TcdB-GTD

The TcdB-GTD Fab B1 complex (called GTD-B1 below) crystallized in the space group of $P2_12_12$ with cell dimensions of a = 210.54, b = 320.08, c = 65.61. The crystals diffracted to 3.59 Å resolution. The final refined model has an R_{free} of 0.258 and R_{factor} of 0.209 with good geometry (Table 4). There are two molecules of GTD-B1 in each asymmetric unit. The refined structural model of the GTD-B1 complex encompasses residues 3–540 of the GTD, 1–218 of the B1 light chain, and residues 1–128 and 136–219 of the B1 heavy chain (Fig. 2A). The secondary structures of the GTD-B1 and representative electron density for regions and residues involved in interactions between GTD and B1 are shown in Fig. 2C and B respectively.

The binding site for B1 is located at the hinge region between the MLD and the catalytic subdomain, with an overall binding area of 466 $Å^2$ contributed by the heavy chain and 329 $Å^2$ contributed by the light chain. The overall binding site involves three loops of the GTD (Fig. 2C). Loop A connects MLD helix 4 with strand 1 of the catalytic sub-domain. Within loop A, P93 forms van der Waals interactions with Y100 from the heavy chain, K96 forms a salt bridge with D101 of the heavy chain, and N97 forms H-bond interactions with L56 and D57 from the light chain (Fig. 2D). Loop B connects helix 5 and strand 2 of catalytic domain; within loop B, S123 interacts with H59 from the light chain, D124 forms an H-bond interaction with Y32 of the heavy chain and with R51 of the light chain, and N126 forms an H-bond interaction with K58 of light chain (Fig. 2E). Loop C connects helix 7 and strand 6; within loop C, the main chain NH and carbonyl of L365 forms H bond interactions with the carbonyl of S31 and NZ of K53, respectively. The side chain of L365 sticks into a hydrophobic pocket formed by Y32, W33, and Y100 of the heavy chain. Considering the extensive interactions with B1 that L365 involves, it may play a critical role in B1 binding (Fig. 2F).

The binding site of B1 includes interactions with both the heavy and light chains. For the heavy chain, all three loops in the variable domain are involved in GTD binding, while for the light chain, only the loop that encompasses residues 55–59 is involved in binding of GTD.

2.3. Structural comparison of TcdB GTD-B2 and TcdB GTD-B1 complexes and with the full-length TcdB

Superposition of the TcdB GTD-B2 and TcdB GTD-B1 complexes based on all α-carbons of the GTD led to a root-mean-square deviation (RMSD) of 0.5A, suggesting the overall conformational change of the GTD upon binding of B1 or B2 is minimal (Fig. 3L). B1 and B2 recognize non-overlapping epitopes away from the catalytic center of the GTD. Structural superposition of TcdB GTD-B1, TcdB GTD-B2 and the full-length TcdB suggests neither B1 nor B2 clashes with any part of TcdB, indicating that B1 and B2 are able to bind the full-length TcdB simultaneously (Fig. 3R).

2.4. Neutralizing activity of a combination of two anti-TcdB mAbs in functional assays in vitro

While individual B1 and B2 mAbs displayed measurable neutralizing activity in the in vitro functional assays, we hypothesized that since these mAbs recognize non-overlapping epitopes within the N-terminal domain of TcdB, their combination might demonstrate synergy and enhanced potency (Anosova et al., 2015). As these mAbs displayed high activity in both the Vero cell cytotoxicity and T84 cell transepithelial electrical resistance (TEER) assays when tested individually, to observe the

synergistic effect of the B1+B2 mAb combination we had to submit this mAb pair to more stringent stress conditions. In the Vero cell assay stress test, neutralizing activity of the individual and the B1+B2 pair mAbs were assessed against increasing TcdB concentrations (4 x, 12 x, 36 x, 108 x, 324 x the 50% maximum cytopathic concentration [MC50]). In the TEER assay, the toxin stress on the mAbs was achieved by increasing the toxin concentration to 20 x TEER50 and extending T84 cell monolayer exposure to the TcdB from 2.5 h (h) to 3.5 h and then to 5 h.

In the Vero assay (Table 1), while the 4 x MC50 concentration of toxin did not allow differentiation between the potency of individual mAbs and their combination, at the 12 x MC50 concentration superior potency of the two mAbs became apparent; individual mAbs completely lost their neutralizing capacity whereas the combination continued to exhibit a potent neutralizing response. Even increasing TcdB concentration further, to the levels found in the gut of symptomatic CDI patients (324 x MC50) (Anosova et al., 2015) did not fully abolish the neutralizing activity of the B1+B2 mAb combination. Likewise, in the TEER assay (Table 2) after 2.5 h of exposure to the toxin, there was minimal difference between the individual mAbs and their combination. However, by 5 h of exposure to the toxin the superiority of the B1+B2 combination over the individual mAbs became obvious. The increases in toxin neutralizing potency for the combination of B1+B2 over equimolar amounts of individual mAbs demonstrates that the function of these two antibodies is not merely additive, but truly synergistic.

To better dissect the contribution of Fc versus Fab regions of the antibodies in this functional synergy, we tested the in vitro neutralizing activity of only Fab regions of these mAbs (Fig. 4). While B1 and B2 Fabs alone exhibited minimal and moderate neutralizing activities respectively in these testing conditions, the combination of B1 and B2 Fabs showed functional synergy exceeding the activity of the B1 and B2 Fabs alone. This synergy is most apparent at the lowest concentrations of Fabs assessed. Thus, similar to the previous results with mAbs, we have observed potentiation of the neutralizing response for the combination of these two Fabs.

2.5. Binding of mAbs to GTD and MLD

As anticipated, both B1 and B2 bind to the recombinant GTD when measured by Biolayer Interferometry (BLI) in real time. Based on a previous finding that a highly conserved "SGRNK" motif of the MLD four-helix bundle abrogates direct binding of the toxin to the cell (Geissler et al., 2012), we measured the binding affinities and kinetic constants of B1 and B2 against the GTD, with and without S66A/R68A mutations. (Table 3). The k_{on} for both mAbs binding to the recombinant GTD was relatively unchanged between the wild-type (WT) and double mutant. While the k_{off} for B1 was also relatively unchanged, the k_{off} for B2 increases 26-fold in the double mutant relative to the WT.

3. Discussion

Monoclonal antibodies B1 and B2 possess potent toxin-neutralizing activity (Anosova et al., 2015) and as such warranted the precise mapping of their binding epitopes by X-ray crystallography. The location of the B2 epitope on the MLD is consistent with peptide binding data from our previous study (Anosova et al., 2015). Although the exact mechanism of B2 neutralization remains undefined, the interactions between B2 and the MLD domain correspond well with the models established by Geissler et al. and Chavez et al. both indicating the importance of loop 1 and loop 3 in membrane association (Geissler et al., 2012; Chavez et al., 2015, 2016; Reinert et al., 2005). Both models indicate the highly conserved basic residues R18 and R68 are important for interactions with PS, membrane localization, and glycosylation activity. In the binding assay, S66A/R68A double mutant TcdB-GTD loses significant binding affinity with B2 compared to the wild type (Table 3). In the GTD-B2 structure, the conformation of R68 is similar to that in the isolated GTD domain structure and is not involved in B2 binding, but rather in maintaining the
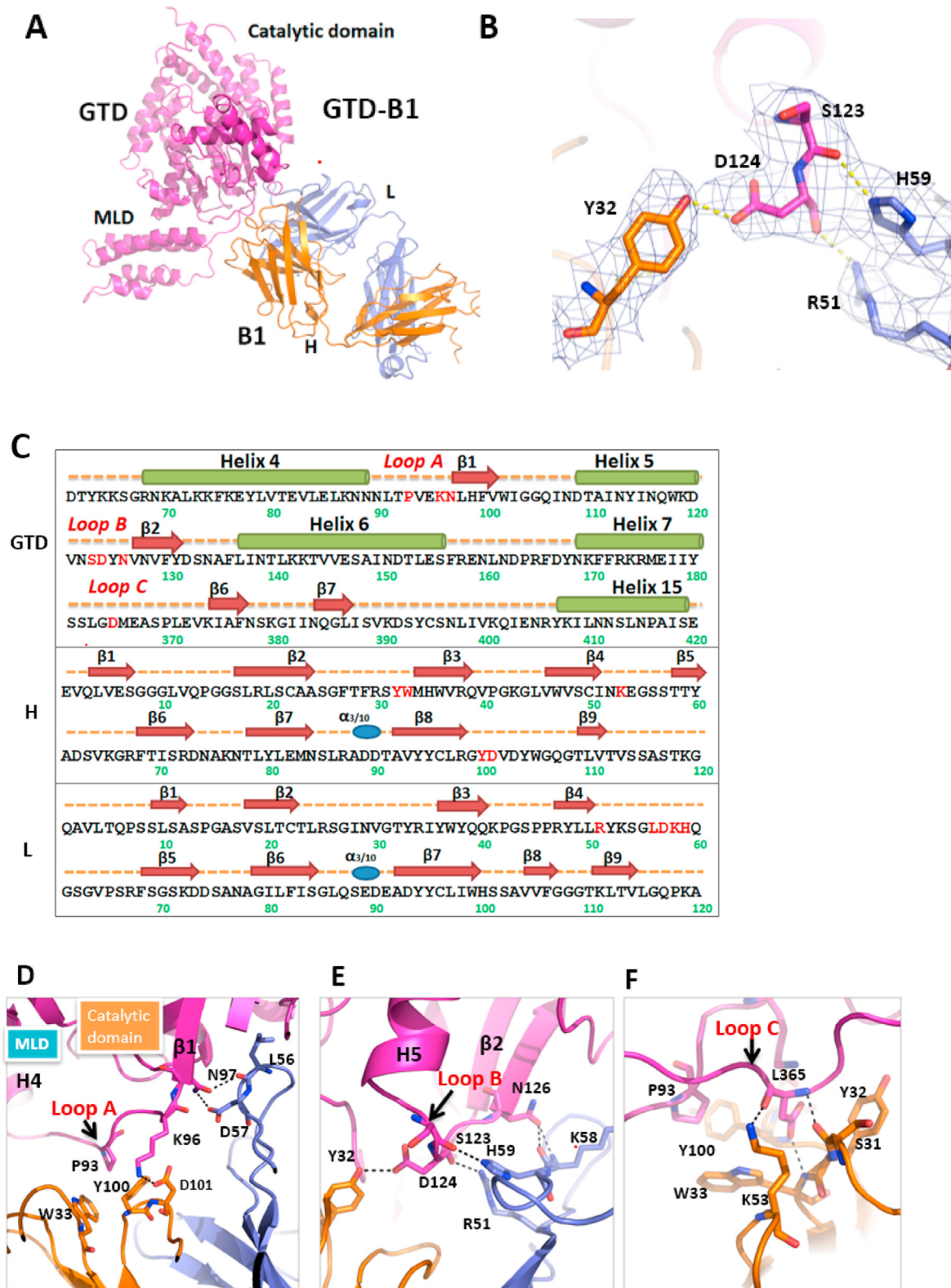
Fig. 2. A: Crystal structure of TcdB GTD -B1. Heavy chain (H) and light chain (L) of B1 are shown in gold and light blue, respectively. GTD is shown in magenta. MLD and catalytic domains of GTD are labeled. B: 2Fo-Fc electron density contoured at 1.0σ for representative residues involved in interactions between H, L chain of B1 and Loop B of GTD. C: Secondary structure schematic representation for GTD, H chain, L chain of B1 for regions involved in interactions. Residues involved in interactions are labeled in red, Loop A Loop B and Loop C are labeled in red. D: Detailed interactions between H, L chain of B1 and Loop A of GTD. E: Detailed interactions between H, L chain of B1 and Loop B of GTD. F: Detailed interactions between H, L chain of B1 and Loop C of GTD. (For interpretation of the references to colour in this figure legend, the reader is referred to the Web version of this article.)
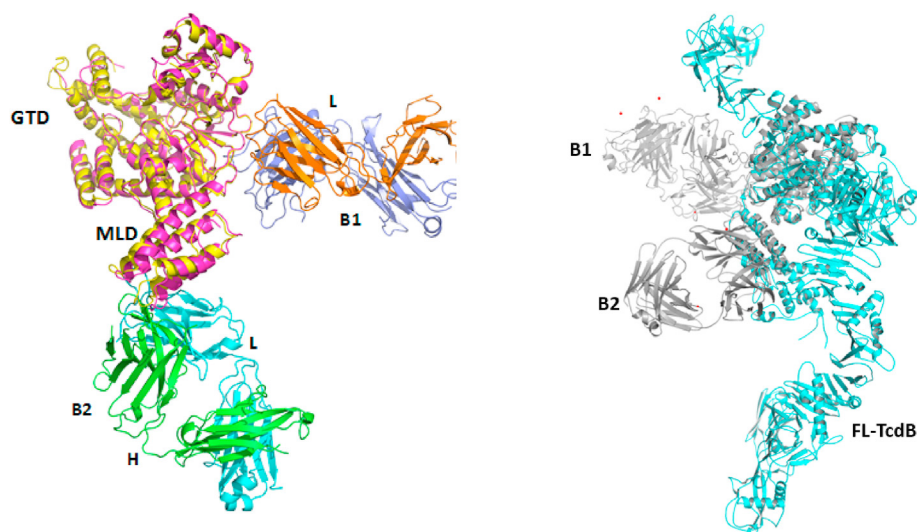
Fig. 3. L: Superposition of GTD-B2 and GTD-B1 complex structures. GTD, Chain H and chain L of GTD-B1 are shown in pink, gold and light blue, respectively. GTD, Chain H and chain L of GTD-B2 are shown in yellow, green and cyan, respectively. R: Superposition of GTD-B1, GTD-B2 complex structures with the full-length TcdB (FL-TcdB) structure. FL-TcdB is shown in cyan, GTD-B1 and GTD-B2 are shown in grey. (For interpretation of the references to colour in this figure legend, the reader is referred to the Web version of this article.)

Table 1

Neutralizing titer and completeness of protection of individual and a combination of two *C. difficile* TcdB-specific mAbs against increasing exposure to *C. difficile* TcdB of toxinotype 0, in Vero cell assay.

mAb/combination	4 x MC50		12 x MC50		36 x MC50		108 x MC50		324 x MC50	
	NT50 (pM)	Max % comp	NT50 (pM)	Max % comp	NT50 (pM)	Max % comp	NT50 (pM)	Max % comp	NT50 (pM)	Max % comp
B1	<33	**95**	>133,333	**0**	ND	**ND**	ND	**ND**	ND	**ND**
B2	<33	**78**	>133,333	**0**	ND	**ND**	ND	**ND**	ND	**ND**
B1+B2	<33	**100**	<67	**90**	107	**91**	>133,333	**46**	>133,333	**14**

Max % comp: Maximum % completeness.
ND: Not Done.
MC50: 50% maximum cytopathic concentration.
NT50: defined as the lowest concentration of antibody that resulted in ≥50% neutralization of cytotoxicity.

Table 2

Neutralizing titer and completeness of protection of individual and a combination of two *C. difficile* TcdB specific mAbs against increasing exposure to *C. difficile* TcdB of toxinotype 0, in T84 cell-based TEER assay.

mAb/combination	2.5 h		3.5 h		5 h	
	NT50 (pM)	Maximum % completeness	NT50 (pM)	Maximum % completeness	NT50 (pM)	Maximum % completeness
B1	583	**83**	759	**81**	2750	**59**
B2	192	**88**	462	**81**	4250	**69**
B1+B2	219	**92**	210	**88**	557	**90**

mAb: monoclonal antibody.
NT50: defined as the lowest concentration of antibody that resulted in ≥50% neutralization of cytotoxicity.
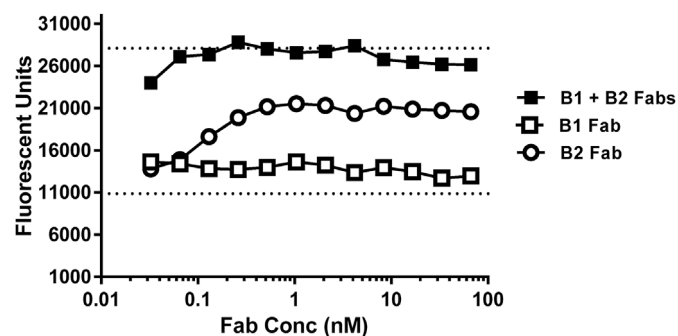
Fig. 4. Neutralizing activity of Fabs of *C. difficile* B1 and B2 TcdB-specific Fabs against *C. difficile* TcdB of toxinotype 0, in Vero cell assay. Fabs were tested at the 4xMC50 concentration of TcdB. The lower dotted line indicates maximum intoxication and upper dotted line shows maximum protection of cell monolayer in the presence of 4xMC50 of TcdB and medium only, respectively.

overall structure of loop 1 where residue F17, Q21, D22, E23 make strong contacts with B2. Similar to R68, R18 is also mainly involved in maintaining the loop 1 structure and forms parallel interaction with R68 and H-bond interaction to E21. These structural observations suggest the loss of membrane association for the R18 and R68 mutants may be due to the overall conformational change of loop 1 which was proposed to be important for membrane association (Geissler et al., 2012; Chavez et al., 2015, 2016; Reinert et al., 2005).

In addition to the essential basic residues in MLD loop 1 and loop 3, Geissler et al. and Chavez et al. also found the highly hydrophobic residues on loop 1 and loop 3 to be associated with strong membrane association. For example, in *Clostridium sordellii* lethal toxin, the F17 mutant was found to strongly decrease the binding to PS and lower the glycosylation rate towards membrane-bound Ras. In the GTD-B2 complex structure, F17 in loop 1 forms a hydrophobic interaction with Y53 of B2.

Localization of the B2 epitope exclusively on loop 1 and loop 3 of the MLD raises the possibility that the neutralizing activity of this mAb might result from masking of the MLD and blockage of GTD membrane

Table 3

Binding kinetics of B1 and B2 mAbs against recombinant TcdB GTD and mutant TcdB GTD, containing the double mutations S66A and R68A.

mAb	TcdB-GTD	K_D (M)	k_{on} (1/Ms)	k_{on} Error	K_{off} (1/s)	K_{off} Error	Full R^2
B1	Wild-type	2.59E-10	2.36E+05	9.24E+02	6.12E-05	1.29E-06	0.9992
B1	Mutant S66A/R68A	2.73E-10	2.66E+05	1.37E+03	7.26E-05	1.67E-06	0.998419
B2	Wild-type	**5.93E-10**	1.53E+05	3.70E+02	**9.07E-05**	7.98E-07	0.999777
B2	Mutant S66A/R68A	**1.48E-08**	1.59E+05	1.64E+03	**2.35E-03**	7.04E-06	0.996022

mAb: monoclonal antibody.

GTD: glucosyltransferase domain.

K_D: equilibrium dissociation constant as k_{on}/k_{off}.

k_{on}: association rate constant.

k_{off}: dissociation rate constants.

Table 4

Data collection and structural refinement statistics for GTD-B1 and GTD-B2. Crystal parameters and data collection statistics are derived from AIMLESS[37]. Refinement statistics were obtained from PHENIX[38]. Data in parentheses correspond to the highest resolution shells.

Data Collection	GTD-B2	GTD-B1
Resolution (Å)	44.43–1.80	74.8–3.59
Space group	$P2_1$	$P2_12_12$
Unit-cell parameters (Å)	a = 61.16	a = 210.54
	b = 110.72	b = 320.08
	c = 83.06	c = 65.61
	$\beta = 99.33°$	
Total reflections	352,755	388,294
Total unique reflections	95,088	53,178
R_{sym}	0.043 (0.466)	0.257 (1.32)
Rmeas	0.06 (0.703)	0.298 (1.544)
Rpim	0.041 (0.475)	0.151 (0.784)
Completeness (%)	93.9 (99.9)	100 (99.9)
Mean (I/σ(I))	14.9(2.3)	8.6 (2.0)
Redundancy	3.7 (3.8)	7.3 (7.3)
CC1/2	0.999(0.704)	0.992(0.635)
Refinement statistics		
R_{work}	0.186	0.209
R_{free}	0.222	0.258
Number of reflections		
Total	95,043	53,077
R_{free}	4684	1998
Model geometry		
R.m.s.d bonds (Å)	0.007	0.003
R.m.s.d angles (°)	1.105	0.73
*Ramachandran distribution**		
Favored (%)	95.52%	89.47
Allowed (%)	3.44%	8.9

localization. This is analogous to the mode of action proposed for the E3 Fab, which was found to bind to a different region of the MLD four-helix bundle in the structure of full-length TcdB (Chen et al., 2019). This hypothesis is in contradiction with the general understanding that most antibodies function on the cell surface, but since the details of the translocation of the GTD from the endosome to the cytosol remain unclear, such a mode of action cannot be ruled out. An alternative explanation is that B2 cannot be translocated into the cytosol due to its large sizes and the neutralization mechanism might be purely due to steric hindrance during GTD translocation.

B1 was found to bind to a novel epitope at the hinge region between the GTD catalytic domain and the MLD domain. The mechanism of B1 neutralization remains to be understood. One possible mechanism is that B1 binding might rigidify TcdB and thereby prevent conformational flexibility between the catalytic and MLD sub-domains of the GTD. Although such conformational flexibility has not been observed so far in current available TcdB structures, and the significance of the conformational flexibility between the catalytic and MLD sub-domains of the GTD has not been established, the fact that B1 mAbs neutralize TcdB through recognizing an epitope in this region leads us to hypothesize such conformational change may occur, potentially when interacting with the

small GTPases during catalysis. This hypothesis is also based on the assumption that B1 can be translocated into the cytosol together with the GTD domain. An alternative explanation is that B1 cannot be translocated into the cytosol due to its large sizes and the neutralization mechanism might be purely due to steric hindrance during GTD translocation.

The mechanism of the synergistic effects of B1 and B2 remains to be determined. Structural superposition between B1, B2 and the full length TcdB indicates B1 and B2 are able to bind the full length TcdB simultaneously without generating a physical clash with other parts of TcdB (Fig. 3R). A likely explanation of the synergistic effects of B1 and B2 is that simultaneous binding to non-overlapping functional epitopes of B1 and B2 leads to the observed synergy. The combination of B1+B2 is not the only pair of synergistic antibodies described in the context of *C. difficile* TcdA & TcdB. Anti-TcdB TLD mAb B4 and anti-TcdB CTD mAb B6 had very limited activity in the Vero-based assay when tested individually, but when combined they exhibited potent neutralization activity (Davies et al., 2013). Similar synergistic effects have been observed by others, for non-overlapping humanized rat mAbs against *C. difficile* TcdB (Davies et al., 2013) and for murine mAbs against TcdA (Demarest et al., 2010). Taken together, these data indicate that synergistic antibodies against non-overlapping epitopes of a single toxin molecule might be considered as a potentially viable strategy for neutralizing *C. difficile* toxin. Although the precise mechanism of the synergistic effect between mAb B1 & B2 has yet to be elucidated, the mere observation of synergy hints at the possibility to develop a single molecule bi-specific mAb therapeutic or prophylactic product with enhanced efficacy against *C. difficile* TcdB as compared to a single monospecific mAb product.

In summary, in this work we have identified two novel and potent mAbs, B1 and B2, targeting the TcdB GTD domain with synergistic effects. Novel non-overlapped epitopes were identified for B1 and B2 through X-ray crystallography and the B2 epitope belongs to a conserved MLD with presumed membrane localization activity. Furthermore, B2 was shown to target key regions of the MLD (loop 1 and loop 3) that are proposed to be essential for membrane localization. To the best of our knowledge, B2 is the first mAb targeting the MLD with epitopes on loop 1 and loop 3 of the MLD and this MLD-targeting strategy of B2 could have broader implication for neutralization of toxins within the conserved MLD domain across the larger LCGT toxin family.

4. Experimental procedures

4.1. Expression and purification of WT and mutant TcdB-GTD proteins

The gene fragment encoding WT TcdB-GTD, corresponding to residues 1–546 of toxinotype 0, was synthesized and subcloned into a pET28a expression vector containing an N-terminal 6xHis tag and TEV protease cleavage site. To construct the S66A/R68A double mutant form of TcdB-GTD, forward and reverse primers introducing the double mutation were used, in combination with pET28a sequencing primers, to create two overlapping fragments carrying both mutations which were combined in a second PCR reaction to recreate the full-length sequence.

Both WT and mutated TcdB-GTD were recombinantly expressed in

BL21 Star (DE3) *E. coli* using the Overnight Express™ Autoinduction System 1 (Novagen, USA) as per the manufacturer's instructions, with the following modification: Overnight seed culture contained 1% glucose in LB media with Kanamycin. Expression was performed for 24 h at 25 °C, 225 rpm. *E. coli* was harvested by centrifugation at 7500 rpm, 30 min at 25 °C and the pellet was frozen at −80 °C until processed for protein purification. At the time of downstream processing the frozen *E. coli* pellet was resuspended in ~10 mL ice cold 50 mM Tris, 0.5 M NaCl, 10–35 mM Imidazole, pH 7.5 (IMAC Buffer A) with 1 x EDTA free protease inhibitor cocktail per g of pellet. Prior to cell disruption by microfluidization, ~0.2 μL of Lysonase™ Bioprocessing Reagent (EMD Millipore, USA) was added per mL of resuspended pellet and cells were mechanically disrupted by 2 passes at 15,000 psi, on ice. Material was clarified by centrifugation at 15,000×*g* for 1 h. The supernatant fraction was loaded onto a 5 mL HisTrap HP chromatography column (GE Healthcare Life Sciences, USA), the resin was washed with 10 column volumes (CV) IMAC Buffer A and proteins were eluted from the resin by linear gradient 0–100% IMAC Buffer B (50 mM Tris, 0.5 M NaCl, 0.5 M Imidazole, pH 7.5) under native conditions. Elution fractions containing the target protein were pooled and concentrated to 2–4 mL on a Vivaspin 30 kDa MWCO centrifugal concentrator (Sartorius, Germany) prior to polishing by size exclusion chromatography on a 65 mL Sephacryl S200 PG column, isocratic elution over 1.5 CV in 50 mM Tris, 0.15 M NaCl, pH 7.5. Peak fractions of the appropriate MW (~64 kDa) were pooled. Material designated for crystallography was further concentrated to ~10 mg/mL by Vivaspin centrifugal concentrator (Sartorius, Germany) and flash frozen on liquid nitrogen prior to storage at −80 °C.

4.2. Expression and purification of WT and mutant TcdB-MLD proteins

Recombinant expression and purification of TcdB-MLD, WT, and mutant proteins was performed similarly to the preparation of the GTD described above, with the following exceptions: Recombinant protein expression was induced by addition of 1 mM Isopropyl β-D-1-thiogalactopyranoside (IPTG) during the exponential phase (OD$_{600}$ 0.6–1.0) of growth and *E. coli* pellet was harvested after 4 h at 37 °C, 225 rpm. Cell disruption was accomplished by sonication (Branson Ultrasonifier Ultrasonic Cell Disruptor (USA) equipped with a microtip) for 2 × 60 s, 50% duty cycle at the microtip limit, on ice. Nickel affinity chromatography was performed in the batch mode using NiNTA resin (QIAGEN, USA). Proteins were polished by bind-and-elute anion exchange chromatography on a HiTrap Q Sepharose HP (GE Healthcare Life Sciences, USA) column. Proteins were bound to the column in 50 mM Tris, 0.1 M NaCl, pH 7.5 and eluted by linear gradient to 50 mM Tris, 1.0 M NaCl, pH 7.5. Elution fractions containing the target protein were pooled, concentrated to ~1.0–3.0 mg/mL by Vivaspin 3 kDa MWCO centrifugal concentrator buffer exchanged to 50 mM Tris, 0.1 M NaCl, pH 7.5 by Zeba desalting column (Thermo Fisher Scientific, USA) and flash frozen on liquid nitrogen prior to storage at −80 °C.

4.3. Preparation of Fab B1 and B2

mAb sequences proprietary to BliNK were synthesized by Invitrogen and cloned into pcDNA3 using standard molecular biology techniques. Stable CHO cell lines were established by methotrexate selection. mAbs were expressed in Opti-CHO medium (Invitrogen, USA) including 4 mM glutamine and captured on MabSelectSure resin (GE Healthcare, USA). mAbs were recovered by elution with 50 mM sodium citrate, pH 3.5, immediately neutralized with 1M Tris base, and dialyzed into DPBS buffer pH 7.2 (Invitrogen, USA). mAbs were concentrated to 5 mg/mL and sterile-filtered. The resulting mAbs were digested and purified to generate Fabs for subsequent structural studies. Briefly, ~50 mg of each mAb (concentration ~ 5 mg/mL) was dialyzed against 1 L of sample buffer (20 mM sodium phosphate, 10 mM EDTA, pH 7.0) overnight at +4 °C in slide-a-lyzer cassettes, 10 kDa MWCO (Thermo Fisher Scientific, USA). Immediately before use, digestion buffer was prepared by addition

of 20 mM cysteine to the sample buffer and adjusting the pH to 7.0. Digestion was performed overnight at 37 °C with agitation using 5 mL immobilized papain resin (Thermo Fisher Scientific, USA) as per the manufacturer's instructions. Following digestion, the Fc portion of the molecule and any undigested mAb was removed from the mixture by batch binding to 1 mL of loose Protein A resin (native Protein A Sepharose FF, GE Healthcare Life Sciences, USA). Purified Fab was concentrated to 2–5 mg/mL by Vivaspin 10 kDa MWCO centrifugal concentrator and buffer exchanged to 20 mM HEPES, 0.2 M NaCl, pH 7.4 by dialysis and then stored at +4 °C for future use. Complete removal of Fc and undigested mAb was confirmed by Western blot detection using Alkaline Phosphatase-conjugated goat α-human IgG (Heavy + Light chain) (Southern Biotech, USA).

4.4. Determination of dissociation constants by Biolayer Interferometry (BLI)

Kinetics for mAbs binding to the TcdB GTD and MLD proteins was performed by BLI using a FortéBio Octet® Red96. WT and mutant mAbs were diluted in kinetic buffer (KB =PBS pH 7.4/0.002% Tween-20/ 0.01% albumin/0.005% sodium azide) to a concentration of 10 μg/mL and immobilized on protein A biosensors at 25 °C with 1000 rpm agitation, then allowed to associate with Tcd-B GTD WT and MLD mutant diluted in KB at 50–2 nM dilution range for 400 s, followed by a dissociation step in KB for 900 s. Data were analyzed using the ForteBio Data Analysis 7.0 software (Pall, USA) using global fitting and a 1:1 binding model to calculate association (k_{on}) and dissociation (k_{off}) rate constants, and the equilibrium dissociation constant (K_D) as k_{on}/k_{off}.

4.5. Vero cell-based C. difficile TcdB neutralization assay

The assay procedure was described in detail previously (Anosova et al., 2015). In brief, Vero cells were seeded at 2.5×10^4 cells/well of a 96-well plate and incubated overnight. Purified *C. difficile* toxinotype 0 TcdB was produced in-house from the reference strain VPI 10463 (ATCC 43255), as per the Sanofi Pasteur manufacturing process. One MC50 dose was 0.016 pM for TcdB. Twofold dilutions of the mAbs were mixed with an equal volume of desired toxin concentrations. There were few orders of magnitude molar excess of mAbs over toxin, even at the lowest concentration of antibody assessed. After 1 h of incubation, medium was removed from 96-well plates containing the Vero cell monolayer, and 100 μL of antibody-toxin mixture was added to the wells. After 72 h of incubation, the cells were washed with phenol red free medium and 100 μL of the medium and 10 μL of AlamarBlue (Invitrogen, USA) were added to each well. The plates were mixed and incubated at 37 °C for 4 h before fluorescence was read at 560–590 nm with a cutoff at 590 nm. The fluorescence results were plotted over antibody concentration. The NT50, which was defined as the lowest concentration of antibody that resulted in 50% neutralization of cytotoxicity, was calculated for each antibody using GraphPad Prism (GraphPad Software, Inc., La Jolla, CA, USA). The calculation of maximum completeness of protection was done as follows: (average mAb fluorescence at upper asymptote–average fluorescence of medium-only control)/(average fluorescence of toxin-only control–average fluorescence of medium-only control) X 100. Testing was performed in at least three separate experiments. Intra-assay precision was 20%.

4.6. Transepithelial electrical resistance (TEER) C. difficile TcdB neutralization assay

The assay procedure was described in detail previously (Anosova et al., 2015). In brief, T84 human colonic carcinoma derived cells (ATCC CCL-248) were seeded into 0.4 μm polyester transwell plates (Corning Costar, USA) at a seeding density of 3.6×10^5 cells/cm^2. The cells were maintained at 37 °C with 5% CO$_2$ in complete culture medium for 10–12 days until stable transepithelial resistance was achieved. Medium was

replaced in both the upper and lower compartments daily from day 6, and on the day of assay. For testing of mAbs neutralizing activity, TcdB was combined with antibody at a 1:1 ratio by volume and incubated at 37 °C for 30 min before being added to polarized T84 cells. TcdB TEER assays were performed by adding TcdB antibody combinations to the lower compartment of the transwell. A final concentration of 1.1 nM toxin B of toxinotype 0 was used for the challenge dose and was equivalent to 20 x TEER50. The controls consisted of at least one well per plate of toxin challenged without antibody and one well containing medium only. Transepithelial resistance was measured immediately (T0) before toxin-antibody sample addition, and then after 2.5–5h (T150-T300) of incubation at 37 °C and 5% CO_2. Percentage TEER loss was calculated using the equation [(T0-T150)/T0] x 100% – %TEER loss in negative well. The percentage protection for antibody was calculated using the equation: (% TEER loss in toxin-only challenge) – (% TEER loss in antibody neutralized toxin challenge). The NT50, which was defined as the lowest concentration of antibody conferring ≥50% protection, was calculated for each antibody using GraphPad Prism (GraphPad Software, Inc., La Jolla, CA, USA). The percentage completeness of protection represents the proportion of toxin-induced damage that was prevented by the highest concentration of mAb. Testing was performed in at least three separate experiments. Intra-assay precision was 20%.

4.7. Crystallography of TcdB GTD Fab complexes

Equimolar amounts of GTD and Fab B2 or B1 were incubated on ice for 2.5 h and the resulting complexes purified by gel filtration on a Superdex S200 10/300 GL column (GE Healthcare Bio- Sciences, Pittsburgh PA, USA) equilibrated in 50 mM Tris pH 7.5, 150 mM NaCl. Peak fractions corresponding to the complex were pooled, concentrated and used in crystallization experiments.

All crystals were grown at 293 K. Crystals of the complex of GTD and FabB1 were generated by microseed-matrix screening (D'Arcy et al., 2007). Original crystals were grown by mixing equal amounts of protein complex at 20 mg/mL and reservoir solution consisting of 0.1 M HEPES pH 7.5, 40% polyethylene glycol 400 and 0.2 M calcium acetate. These crystals were resuspended in 50 μL of reservoir solution, crushed with a seed bead (Hampton Research, Aliso Viejo, CA), and used for seeding into drops consisting of equal amounts of protein complex at 10 mg/mL and reservoir consisting of 0.1 M sodium cacodylate pH 5.0, 40% PEG 300 and 0.2 M calcium acetate. Crystals were frozen directly in liquid nitrogen. Crystals of the complex of GTD and Fab B2 were grown by mixing equal amounts of protein complex at 15 mg/mL and reservoir consisting of 0.1 M TRIS pH 8.2 and 39% polyethylene glycol 400. Crystals were frozen directly in liquid nitrogen.

4.8. Data collection, structure determination and analysis

The diffraction data were collected at 100 K at the APS LS-CAT 21-ID-D beamline using an EIGER 9M detector (Dectris, Switzerland). The data were then integrated with XDS and scaled using AIMLESS (Kabsch, 2010a; Evans and Murshudov, 2013) (Table 4). The structure of the GTD-B2 and GTD-B1 was determined by molecular replacement with the program Phenix (Adams et al., 2010) using the atomic coordinates of the Fab Fragment 3D69 (PDB code) and the published TcdB-GTD (PDB code 2BVL) as the search models. The resulting model was further rebuilt in COOT (Emsley et al., 2010) and refined with Phenix (Table 4). The refined structures were visualized with PyMOL (http://www.pymol.org/). Structures were deposited into the Brookhaven Protein DataBank (PDB ID 7SO7 for B1, 7SO5 for B2).

Credit author statement

Jinyu Liu: Writing- Original draft preparation, Data curation. Michael Kothe, Data curation, Writing- Reviewing and Editing. Jianxin Zhang: Data curation. Eliud Oloo: Data curation. Svetlana Stegalkina: Data curation. Sophia T. Mundle: Data curation, Writing- Reviewing and Editing. Lu Li: Data curation. Jinrong Zhang: Data curation. Leah E. Cole: Data curation. Lucianna Barone: Data curation. Hans-Peter Biemann: Supervision, Writing- Reviewing and Editing, Harry Kleanthous: Data curation. Natalie G. Anosova: Data curation, Writing- Reviewing and Editing. Stephen F. Anderson: Supervision, Writing- Original draft preparation.

Declaration of competing interest

The authors declare that they have no known competing financial interests or personal relationships that could have appeared to influence the work reported in this paper.

References

Adams, P.D., Afonine, P.V., Bunkoczi, G., Chen, V.B., Davis, I.W., Echols, N., Headd, J.J., Hung, L.W., Kapral, G.J., Grosse-Kunstleve, R.W., McCoy, A.J., Moriarty, N.W., Oeffner, R., Read, R.J., Richardson, D.C., Richardson, J.S., Terwilliger, T.C., Zwart, P.H., 2010. PHENIX: a comprehensive Python-based system for macromolecular structure solution. Acta Crystallogr D Biol Crystallogr 66, 213–221.

Albesa-Jove, D., Bertrand, T., Carpenter, E.P., Swain, G.V., Lim, J., Zhang, J., Haire, L.F., Vasisht, N., Braun, V., Lange, A., von Eichel-Streiber, C., Svergun, D.I., Fairweather, N.F., Brown, K.A., 2010. Four distinct structural domains in Clostridium difficile toxin B visualized using SAXS. J. Mol. Biol. 396, 1260–1270.

Anosova, N.G., Cole, L.E., Li, L., Zhang, J., Brown, A.M., Mundle, S., Ray, S., Ma, F., Garrone, P., Bertraminelli, N., Kleanthous, H., Anderson, S.F., 2015. A combination of three fully human toxin A- and toxin B-specific monoclonal antibodies protects against challenge with highly virulent epidemic strains of Clostridium difficile in the hamster model. Clin. Vaccine Immunol. 22, 711–725.

Chavez, C.V., Hoos, S., Haustant, G.M., Chenal, A., England, P., Blondel, A., Pauillac, S., Lacy, D.B., Popoff, M.R., 2015. The catalytic domains of Clostridium sordellii lethal toxin and related large clostridial glucosylating toxins specifically recognize the negatively charged phospholipids phosphatidylserine and phosphatidic acid. Cell Microbiol. 17, 1477–1493.

Chavez, C.V., Haustant, G.M., Baron, B., England, P., Chenal, A., Pauillac, S., Blondel, A., Popoff, M.R., 2016. The tip of the four N-terminal α-helices of Clostridium sordellii lethal toxin contains the interaction site with membrane phosphatidylserine facilitating small GTPases glucosylation. Toxins 8, 90.

Chen, P., Lam, K.H., Liu, Z., Mindlin, F.A., Chen, B., Gutierrez, C.B., Huang, L., Zhang, Y., Hamza, T., Feng, H., Matsui, T., Bowen, M.E., Perry, K., Jin, R., 2019 Aug. Structure of the full-length Clostridium difficile toxin B. Nat. Struct. Mol. Biol. 26 (8), 712–719. https://doi.org/10.1038/s41594-019-0268-0. Epub 2019 Jul 15.

Chumbler, N.M., Rutherford, S.A., Zhang, Z., Farrow, M.A., Lisher, J.P., Farquhar, E., Giedroc, D.P., Spiller, B.W., Melnyk, R.A., Lacy, D.B., 2016. Crystal structure of Clostridium difficile toxin A. Nat Microbiol 1, 15002.

D'Arcy, A., Villard, F., Marsh, M., 2007. An automated microseed matrix-screening method for protein crystallization. Acta Crystallogr D Biol Crystallogr 63, 550–554.

D'Urzo, N., Malito, E., Biancucci, M., Bottomley, M.J., Maione, D., Scarselli, M., Martinelli, M., 2012. The structure of Clostridium difficile toxin A glucosyltransferase domain bound to Mn2+ and UDP provides insights into glucosyltransferase activity and product release. FEBS J. 279, 3085–3097.

Davies, N.L., Compson, J.E., Mackenzie, B., O'Dowd, V.L., Oxbrow, A.K., Heads, J.T., Turner, A., Sarkar, K., Dugdale, S.L., Jairaj, M., Christodoulou, L., Knight, D.E., Cross, A.S., Herve, K.J., Tyson, K.L., Hailu, H., Doyle, C.B., Ellis, M., Kriek, M., Cox, M., Page, M.J., Moore, A.R., Lightwood, D.J., Humphreys, D.P., 2013. A mixture of functionally oligoclonal humanized monoclonal antibodies that neutralize Clostridium difficile TcdA and TcdB with high levels of in vitro potency shows in vivo protection in a hamster infection model. Clin. Vaccine Immunol. 20, 377–390.

Demarest, S.J., Hariharan, M., Elia, M., Salbato, J., Jin, P., Bird, C., Short, J.M., Kimmel, B.E., Dudley, M., Woodnutt, G., Hansen, G., 2010. Neutralization of Clostridium difficile toxin A using antibody combinations. mAbs 2, 190–198.

Emsley, P., Lohkamp, B., Scott, W.G., Cowtan, K., 2010. Features and development of coot. Acta Crystallogr D Biol Crystallogr 66, 486–501.

Evans, P.R., Murshudov, G.N., 2013. How good are my data and what is the resolution. Acta Crystallogr. D69, 1204–1214.

Furuya-Kanamori, L., Marquess, J., Yakob, L., Riley, T.V., Paterson, D.L., Foster, N.F., Huber, C.A., Clements, A.C., 2015. Asymptomatic Clostridium difficile colonization: epidemiology and clinical implications. BMC Infect. Dis. 15, 516.

Geissler, B., Ahrens, S., Satchell, K.J., 2012. Plasma membrane association of three classes of bacterial toxins is mediated by a basic-hydrophobic motif. Cell Microbiol. 14, 286–298.

Genisyuerek, S., Papatheodorou, P., Guttenberg, G., Schubert, R., Benz, R., Aktories, K., 2011. Structural determinants for membrane insertion, pore formation and translocation of Clostridium difficile toxin B. Mol. Microbiol. 79, 1643–1654.

Greco, A., Ho, J.G., Lin, S.J., Palcic, M.M., Rupnik, M., Ng, K.K., 2006. Carbohydrate recognition by Clostridium difficile toxin A. Nat. Struct. Mol. Biol. 13, 460–461.

Hall, I., O'Toole, E., 1935. Intestinal flora of newborn infants. Am. J. Dis. Child. 49, 390–402.

Hernandez, L.D., Kroh, H.K., Hsieh, E., Yang, X., Beaumont, M., Sheth, P.R., DiNunzio, E., Rutherford, S.A., Ohi, M.D., Ermakov, G., Xiao, L., Secore, S., Karczewski, J., Racine, F., Mayhood, T., Fischer, P., Sher, X., Gupta, P., Lacy, D.B., Therien, A.G., 2017. Epitopes and mechanism of action of the Clostridium difficile toxin A-neutralizing antibody actoxumab. J. Mol. Biol. 429, 1030–1044.

Ho, J.G., Greco, A., Rupnik, M., Ng, K.K., 2005. Crystal structure of receptor-binding C-terminal repeats from Clostridium difficile toxin A. Proc. Natl. Acad. Sci. U. S. A. 102, 18373–18378.

Just, I., Selzer, J., Wilm, M., von Eichel-Streiber, C., Mann, M., Aktories, K., 1995. Glucosylation of Rho proteins by Clostridium difficile toxin B. Nature 375, 500–503.

Kabsch, W., 2010. XDS. Acta Cryst. D66, 125–132.

Kroh, H.K., Chandrasekaran, R., Rosenthal, K., Woods, R., Jin, X., Ohi, M.D., Nyborg, A.C., Rainey, G.J., Warrener, P., Spiller, B.W., Lacy, D.B., 2017. Use of a neutralizing antibody helps identify structural features critical for binding of Clostridium difficile toxin TcdA to the host cell surface. J. Biol. Chem. 292, 14401–14412.

Kroh, H.K., Chandrasekaran, R., Zhang, Z., Rosenthal, K., Woods, R., Jin, X., Nyborg, A.C., Rainey, G.J., Warrener, P., Melnyk, R.A., Spiller, B.W., Lacy, D.B., 2018 Jan 19. A neutralizing antibody that blocks delivery of the enzymatic cargo of *Clostridium difficile* toxin TcdB into host cells. J. Biol. Chem. 293 (3), 941–952. https://doi.org/10.1074/jbc.M117.813428. Epub 2017 Nov 27.

Lawson, P.A., Citron, D.M., Tyrrell, K.L., Finegold, S.M., 2016. Reclassification of Clostridium difficile as Clostridioides difficile (Hall and O'Toole 1935) prevot 1938. Anaerobe 40, 95–99.

Lessa, F.C., Mu, Y., Bamberg, W.M., Beldavs, Z.G., Dumyati, G.K., Dunn, J.R., Farley, M.M., Holzbauer, S.M., Meek, J.I., Phipps, E.C., Wilson, L.E., Winston, L.G., Cohen, J.A., Limbago, B.M., Fridkin, S.K., Gerding, D.N., McDonald, L.C., 2015. Burden of Clostridium difficile infection in the United States. N. Engl. J. Med. 372, 825–834.

Manse, J.S., Baldwin, M.R., 2015. Binding and entry of Clostridium difficile toxin B is mediated by multiple domains. FEBS Lett. 589, 3945–3951.

Murase, T., Eugenio, L., Schorr, M., Hussack, G., Tanha, J., Kitova, E.N., Klassen, J.S., Ng, K.K., 2014. Structural basis for antibody recognition in the receptor-binding domains of toxins A and B from Clostridium difficile. J. Biol. Chem. 289, 2331–2343.

Olling, A., Goy, S., Hoffmann, F., Tatge, H., Just, I., Gerhard, R., 2011. The repetitive oligopeptide sequences modulate cytopathic potency but are not crucial for cellular uptake of Clostridium difficile toxin A. PLoS One 6, e17623.

Orth, P., Xiao, L., Hernandez, L.D., Reichert, P., Sheth, P.R., Beaumont, M., Yang, X., Murgolo, N., Ermakov, G., DiNunzio, E., Racine, F., Karczewski, J., Secore, S., Ingram, R.N., Mayhood, T., Strickland, C., Therien, A.G., 2014. Mechanism of action and epitopes of Clostridium difficile toxin B-neutralizing antibody bezlotoxumab revealed by X-ray crystallography. J. Biol. Chem. 289, 18008–18021.

Peterfreund, G.L., Vandivier, L.E., Sinha, R., Marozsan, A.J., Olson, W.C., Zhu, J., Bushman, F.D., 2012. Succession in the gut microbiome following antibiotic and antibody therapies for Clostridium difficile. PLoS One 7, e46966.

Pruitt, R.N., Chagot, B., Cover, M., Chazin, W.J., Spiller, B., Lacy, D.B., 2009. Structure-function analysis of inositol hexakisphosphate-induced autoprocessing in Clostridium difficile toxin A. J. Biol. Chem. 284, 21934–21940.

Pruitt, R.N., Chambers, M.G., Ng, K.K., Ohi, M.D., Lacy, D.B., 2010. Structural organization of the functional domains of Clostridium difficile toxins A and B. Proc. Natl. Acad. Sci. U. S. A. 107, 13467–13472.

Puri, A.W., Lupardus, P.J., Deu, E., Albrow, V.E., Garcia, K.C., Bogyo, M., Shen, A., 2010. Rational design of inhibitors and activity-based probes targeting Clostridium difficile virulence factor TcdB. Chem. Biol. 17, 1201–1211.

Reineke, J., Tenzer, S., Rupnik, M., Koschinski, A., Hasselmayer, O., Schrattenholz, A., Schild, H., von Eichel-Streiber, C., 2007. Autocatalytic cleavage of Clostridium difficile toxin B. Nature 446, 415–419.

Reinert, D.J., Jank, T., Aktories, K., Schulz, G.E., 2005. Structural basis for the function of Clostridium difficile toxin B. J. Mol. Biol. 351, 973–981.

Shen, A., Lupardus, P.J., Gersch, M.M., Puri, A.W., Albrow, V.E., Garcia, K.C., Bogyo, M., 2011. Defining an allosteric circuit in the cysteine protease domain of Clostridium difficile toxins. Nat. Struct. Mol. Biol. 18, 364–371.

Testore, G.P., Nardi, F., Babudieri, S., Giuliano, M., Di Rosa, R., Panichi, G., 1986. Isolation of Clostridium difficile from human jejunum: identification of a reservoir for disease? J. Clin. Pathol. 39, 861–862.

von Eichel-Streiber, C., Boquet, P., Sauerborn, M., Thelestam, M., 1996. Large clostridial cytotoxins–a family of glycosyltransferases modifying small GTP-binding proteins. Trends Microbiol. 4, 375–382.

Yuan, P., Zhang, H., Cai, C., Zhu, S., Zhou, Y., Yang, X., He, R., Li, C., Guo, S., Li, S., Huang, T., Perez-Cordon, G., Feng, H., Wei, W., 2015. Chondroitin sulfate proteoglycan 4 functions as the cellular receptor for Clostridium difficile toxin B. Cell Res. 25, 157–168.

Zhang, Z., Park, M., Tam, J., Auger, A., Beilhartz, G.L., Lacy, D.B., Melnyk, R.A., 2014. Translocation domain mutations affecting cellular toxicity identify the Clostridium difficile toxin B pore. Proc. Natl. Acad. Sci. U. S. A. 111, 3721–3726.